INL/JOU-20-59039-Revision-0

a-U and ?-UZr2 in neutron irradiated U-10Zr annular metallic fuel

December 2020

Tiankai Yao, Luca Capriotti, Xiang Liu, Yachun Wang, Fei Teng, Daniel J Murray, Jian Gan, Michael T Benson, Lingfeng He, Jason M. Harp, Alexander J Winston

Changing the World's Energy Future

INL/JOU-20-59039-Revision-0

a-U and ?-UZr2 in neutron irradiated U-10Zr annular metallic fuel

Tiankai Yao, Luca Capriotti, Xiang Liu, Yachun Wang, Fei Teng, Daniel J Murray, Jian Gan, Michael T Benson, Lingfeng He, Jason M. Harp, Alexander J Winston

December 2020

Idaho National Laboratory
Idaho Falls, Idaho 83415

http://www.inl.gov

Prepared for the
U.S. Department of Energy
Under DOE Idaho Operations Office
Contract DE-AC07-05ID14517

α-U and ω-UZr_2 in Neutron Irradiated U-10Zr Annular Metallic Fuel

Tiankai Yao[a], Luca Capriotti[a], Jason M. Harp[b], Xiang Liu[a], Yachun Wang[a], Fei Teng[a], Daniel J. Murray[a], Alex J. Winston[a], Jian Gan[a], Michael T. Benson[a*], Lingfeng He[a*]

[a]*Idaho National Laboratory, Idaho Falls, ID 83415, USA*
[b]*Oak Ridge National Laboratory, Oak Ridge, TN 37831, USA*
**corresponding authors: Michael.Benson@inl.gov; Lingfeng.He@inl.gov*

Abstract: To develop metallic fuel with ultra-high burnup of 30%-40%, an annular U-10Zr fuel with 55% smear density was fabricated through a casting route and irradiated at the Advanced Test Reactor at Idaho National Laboratory. The annular fuel design also serves as a demonstration of the feasibility to replace the sodium bond with a helium bond to benefit the geological disposal of irradiated fuel, cut the cost of fuel fabrication, and boost the overall metallic fuel economy. This paper reports the results from transmission electron microscopy (TEM) based post-irradiation examination of this fuel type irradiated to a burnup of 3.3% fissions per initial heavy metal atoms. The low burnup was planned for initial screening of this fuel design. After irradiation, the initial U-10Zr microstructure separated into an α-U annular region and an UZr_{2+x} center region with a nanoscale spinodal decomposed microstructure. Because of the large amount of interface areas created in this microstructure, the fission gas atoms and vacancies generated in the UZr_{2+x} phase are possibly pinned at the interface areas, leading to ~20 times smaller fission gas bubbles than those in the neighboring α-U. The large bubbles in α-U become connected and merged into large pores that provide fast paths for fission gas release into capsule plenum which prevents further swelling of fuel slug. The fuel slug center still has open space to accommodate further fuel swelling from solid fission products at higher burnup. Other neutron irradiation induced phase and microstructure change are also characterized and compared with traditional solid fuel designs.

Keywords: Metallic fuel; Swelling; Microstructure; Spinodal decomposition; Radiation damage; Annular Fuel

1. Introduction

The development and application of metallic fuel in the United States dates back to the very early stage of the nuclear era [1]. Metallic fuel served multiple purposes, including plutonium management, energy production, and neutron generation in research reactors. Its recent development is often driven by economic concerns, such as targeting higher burnup to improve overall fuel economy [2]. Initial metallic fuel designs attempted to irradiate solid fuel slugs that were tightly bonded to their cladding, but fission gas-induced swelling lead to cladding breaches at burnups below 3% fissions per initial heavy metal atom (FIMA) due to fuel-cladding mechanical interaction. Further development lead to various new concepts, including decreased smear density[a] and an increased plenum size to accommodate fission gas release [3]. These developments culminated in qualified fuel for the Experimental Breeder Reactor II (EBR-II) that had a burnup limit of 10% FIMA for U-10Zr, and there were successful irradiations of some EBR-II U-20Pu-Zr and U-10Zr fuel pins to ~20% FIMA [4, 5]. High burnup compatibility and other advantages such as straightforward remote fabrication, high uranium (U) density, and favorable characteristics for enabling passive reactor safety position U-Zr based metallic fuel as a leading candidate fuel form for next generation sodium-cooled fast reactors (SFR).

To further improve fuel performance, a sodium free annular fuel design has been developed by Idaho National Laboratory (INL) under US Department of Energy Advanced Fuels Campaign (AFC), targeting an ultrahigh burnup goal of close to 30% FIMA. The annular shape decreased the fuel smear density to 55% which allows inward swelling under the mechanical constrains from cladding and is adequate to accommodate both fission gas-driven swelling and solid fission

[a] smear density of a fuel is the area percentage of actual fuel on fuel cross section

product swelling that impacts higher smear density fuel above 10% FIMA. Since the fuel is bonded directly with the cladding, the sodium bond is eliminated, which simplifies the waste handling associated with sodium disposal [6, 7].

To experimentally validate this novel metallic fuel concept, multiple fuel pins of U-10Zr (wt.%) composition were cast into an annular shape and irradiated at the Advanced Testing Reactor (ATR) at INL. Some of the pins have been removed from the reactor at low burnup. After insertion into ATR, it was found that the cladding did not have uniform inner walls, creating larger gaps between the fuel and cladding than anticipated, creating higher peak inner cladding temperatures than expected. Due to this, the experiments were pulled from the reactor early, allowing them to be used for initial screening of the annular fuel design. [8, 9]. The programmatic designation for the specific fuel pin investigated in this study is AFC-3A R4. Post-irradiation examination (PIE) of this pin shows the microstructure was significantly altered during irradiation [8]. The original annular region is depleted in Zr and became highly porous, while the center part is much denser and enriched in Zr.

In the past several years, focused ion beam (FIB) sample preparation has been widely used to prepare site specific TEM samples with a typical size of 10 x 10 μm instead of using 3 mm discs prepared by conventional methods. The small sample volume significantly decreases sample activity and facilitates TEM based research on irradiated nuclear fuel [10]. Compared with a conventional PIE study based on scanning electron microscopy (SEM) and X-ray diffraction (XRD), TEM provides wholescale characterization of a small volume, including phase, chemical composition, and microstructure information simultaneously, using high flux electron beam at a spatial resolution down to sub-nm scales. Some features of irradiated fuel, such as the phase of heavily damaged fuel matrix material, can be well characterized but impossible to resolve based on XRD patterns due to peak broadening and high background noise.

It was anticipated that the as-cast U-10Zr microstructure should be a dual phase of α-U and δ-UZr_2, based on the phase diagram [11]. The XRD patterns of these two phases, however, are severely overlapped, preventing identification of both phases [12]. Numerous studies can only confidently identify α-U, the volumetrically dominant phase, through this method. Under SEM, the microstructure appears to have laminated layers with alternatively Zr rich and poor at sizes below 1 μm scale. Only through TEM can the phases be identified. A lamella structure of interlaced α-U and δ-UZr_2 with close crystallographic orientation was clearly revealed by electron diffraction pattern [13].

This study presents a detailed phase identification of an irradiated U-10Zr annular fuel from TEM electron diffraction pattern indexing guided by composition analysis from scanning transmission electron microscopy energy dispersive X-ray spectroscopy (STEM-EDS) mapping. These results are compared to PIE from the more thoroughly studied solid, sodium-bonded U-Zr metallic fuel system. The implications of the current study for future annular fuel design and fabrication are also provided.

2. Experiment

The fuel pin for this irradiation experiment was directly cast into annular shape using quartz tubes [14]. Before casting, the tubes were dip coated with ZrO_2 to facilitate post casting separation of the fuel and tube. Due to this, a Zr-rich region formed on both the inner and outer surface of the fuel pin due to chemical reaction between the molten U-10Zr and ZrO_2. For the irradiation experiments, the cast annular fuel slugs were slip fit into the cladding tube and filled with He gas. The full fabrication details for the AFC-3A R4 fuel pin can be found in an INL report [15], and the irradiation details can be found in a previous study [8].

TEM samples were prepared by FIB technique (hereafter being referred as FIB-TEM sample) using a FEI Quanta 3D SEM/FIB dual beam system. Ga ion beams of various energy and current

were used during trenching and lift-out. Final thinning was done using a 5 keV and 48 pA to locally perforate the sample followed by a final polishing using a Ga ion beam of 2 keV and 27 pA. To avoid oxidation, the sample was unloaded from FIB, surveyed, and quickly loaded into the Talos TEM equipped with a field emission gun operated at 200 kV. STEM-EDS was collected using a Super-X EDS System based on ChemiSTEM technology. The STEM-EDS data was collected from an energy range from 0 to 40 keV. Phase identification was primarily carried out based on the indexing of selected area diffraction patterns (SAED).

3. Results

3.1. SEM based PIE

Irradiated U-10Zr annular fuel shows significant fuel restructuring as shown in Figure 1. A more detailed view of the radial microstructure region from the red box on the cross section shown in Figure 1a is shown in Figure 1b. The annulus was occupied by a tertiary phase with moving front lines whose curvature indicates an inwards swelling of the annular fuel during in-pile irradiation. Limited but appreciable remaining open space is found in the center. The relative distribution of elements of interest along a radius defined by the purple line shown in Figure 1b shows four distinguishable regions that each have specific dominant elements. The HT-9 cladding region is dominated by iron (Fe) and chromium (Cr). The outer fuel region is primarily U that is depleted of Zr with dimensions closely matching the original annular fuel before irradiation. Moving towards the fuel center, a region was identified with U concentrations below the original U-10Zr composition and with elevated levels of Zr. Between the outer fuel region and the center region is a 200 μm width interface with a high concentration of Zr and Si. Other elements, such as Nd and Cs, show even distribution inside the fuel region except for pore/void/gap sites.

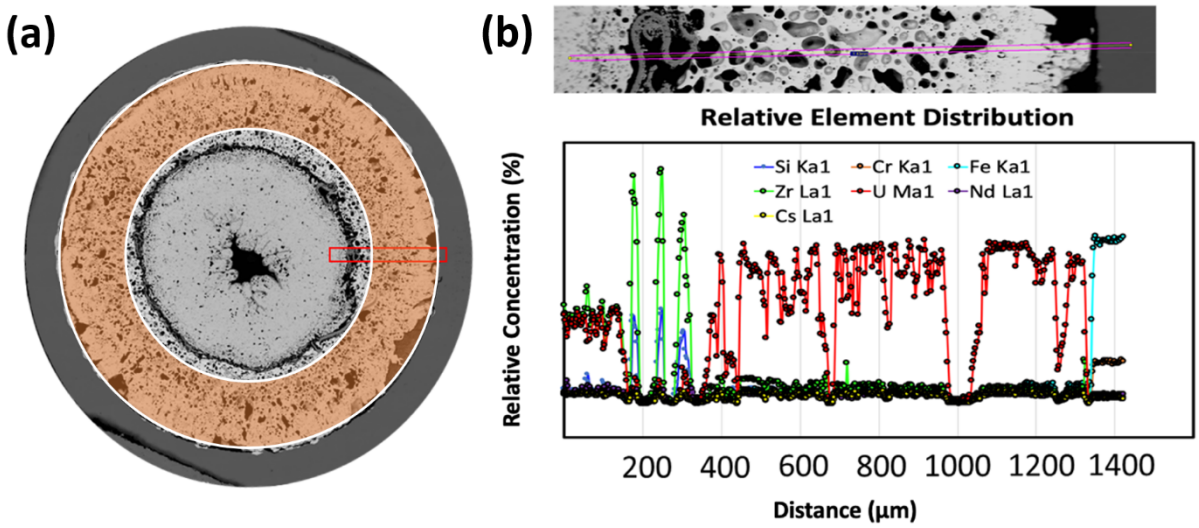

Figure 1. Overview of annular U-10Zr fuel irradiated to 3.3 % FIMA showing an annular region and a central region. Element distribution across the two regions and into the cladding is shown on the lower right. The original fuel cross section before irradiation is highlighted by the orange colored region.

Based on the SEM EDS data, a scheme of fuel regions was color coded and superimposed on the fuel cross section as shown in Figure 2. The red region is HT-9 cladding, the purple region is the fuel outer radial region, and the faint pink region is the fuel inner radial region. Locations for seven FIB-TEM samples are highlighted by white bands with each representing a different region for microstructure characterization and phase identification.

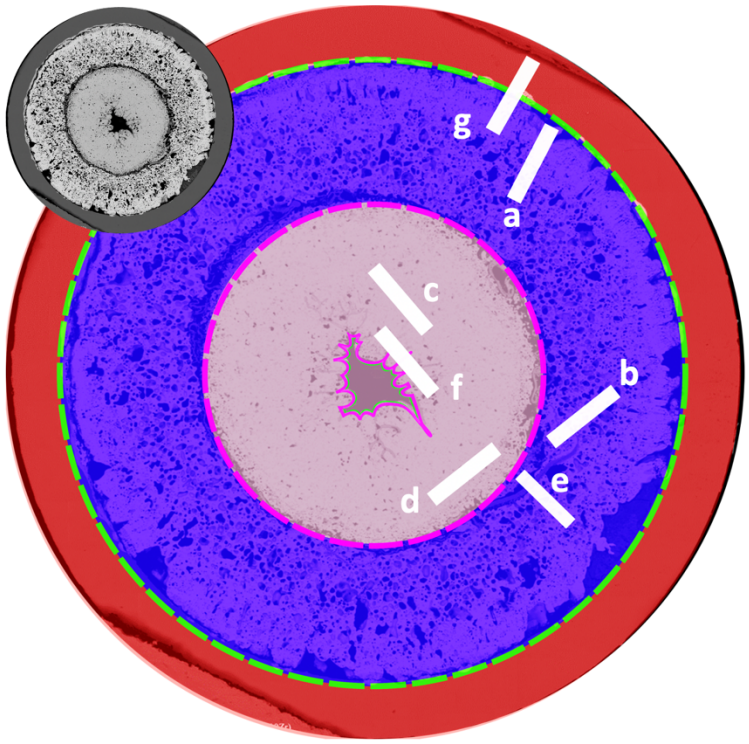

Figure 2. A region scheme superimposed on top of fuel section shown in Figure 1. White bands indicate the regions where FIB-TEM samples have been lifted for different characterization purpose, including Fe infiltration (a), nano Zr clusters (b), omega phase in γ matrix (c), spinodal decomposed microstructure (d), two phase α-γ interface (e), the Zr rind near fuel center (f), and the Zr rind (g). Red, purple, and pink regions represent HT-9 cladding, fuel outer radial region, and fuel center radial region, respectively. The green dotted line represents the fuel-cladding interface and the pink dotted line represents the Zr-Si rich interface between the central and outer radial regions.

3.2. Fuel outer radial region

Figure 3 shows the fuel-cladding interface, color coded the same as in Figure 2. In this region, U is the dominant element. In the outer fuel region very near to the cladding, fission gas bubbles are appreciably smaller than regions further towards the fuel center, and they form a line array perpendicular to the fuel cladding interface. SEM EDS results shows this region has the composition U-3Zr-13Fe, indicating an Fe infiltration from the cladding into the fuel. The infiltration stopped at site 2 with 97U-3Zr at.%. Much further into the U fuel side at site 3, the Zr concentration increase to 7 at.%, but this is still well below the starting composition of U-23Zr

150 at.%.

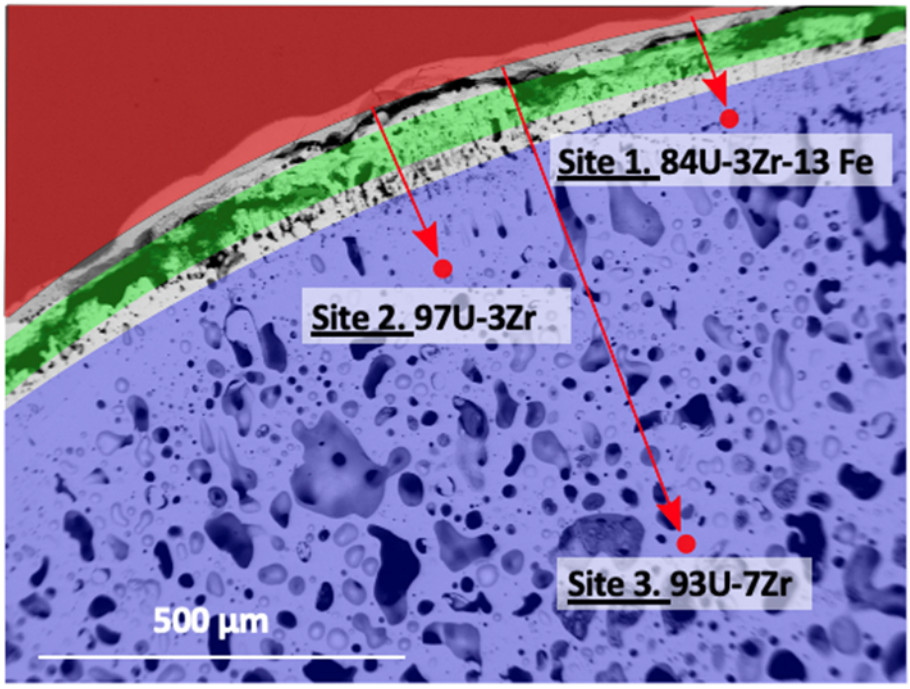

151
152 Figure 3. The variation of major chemical compositions inside fuel near the fuel-cladding
153 interface.
154

155 Two lamellae were prepared in this region: one is near site 1 (Figure 3) in the fuel side
156 (Figure 2, lamella a) and is discussed in Section 3.2.1, while the other lamella was lifted from the
157 region further into fuel center near the boundary between the inner and outer fuel regions (Figure
158 2, lamella b), and is discussed in Section 3.2.2.

159 3.2.1. Iron infiltration

160 The lamella location labeled ‘a’ in Figure 2a indicates the fuel-cladding region that was
161 selected for FIB lift out to investigate Fe infiltration into the fuel. The fuel in this region shows a
162 distinctive columnar grain shape, which is a typical phenomenon for grains inside the diffusion
163 region in diffusion couple studies [16] (see Figure 4d). The distribution of sub-micron sized
164 pores apparently follows the line of grain boundaries (Figure 4b). The TEM bright field (BF)
165 image reveals line features inside the columnar grains, due to enrichment in Fe (Figure 4i).

SAED patterns indicate the dominant phase is α-U with U_6Fe as a secondary phase sharing crystallographic orientations. The [03] zone axis of ideal α-U coincides with the [203] and [13] zone axis of U_6Fe with interplanar distances for (131) of α-U, (512) and (32), both for U_6Fe, being 0.153, 0.146, and 0.159 nm, respectively.

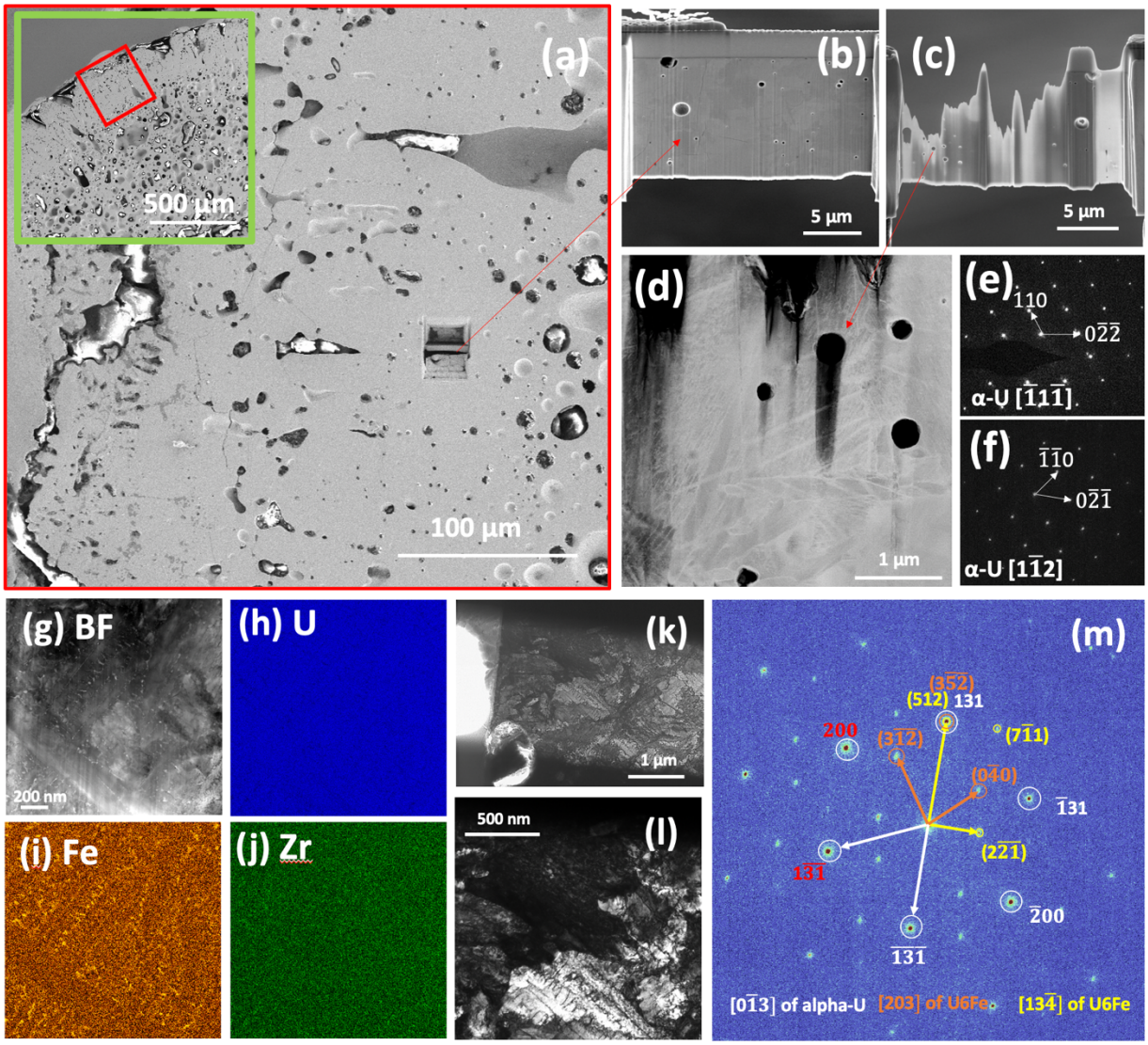

Figure *1*. (a) SEM of the fuel-cladding interface. The region in the red box shows refined gas bubbles < 1 µm near the fuel-cladding interface. (b) and (c) shows FIB-TEM sample preparation before and after thinning. (d) shows typical columnar grains observed in a diffusion couple experiment. TEM SAED pattern indexing ((e) and (f)) indicates the major phase is α-U. A localized region (g) is found to have a dominant α-U phase with a minor phase of U_6Fe STEM EDS mapping ((g) is BF image, (h) shows U map, (i) shows Fe map, and (j) shows Zr map)

indicates iron infiltration formed a pattern inside the α-U matrix. The crystallographic orientation between the U_6Fe phase and the U matrix was revealed by TEM imaging (k-l) and diffraction pattern (m).

3.2.2. Nano Zr clusters.

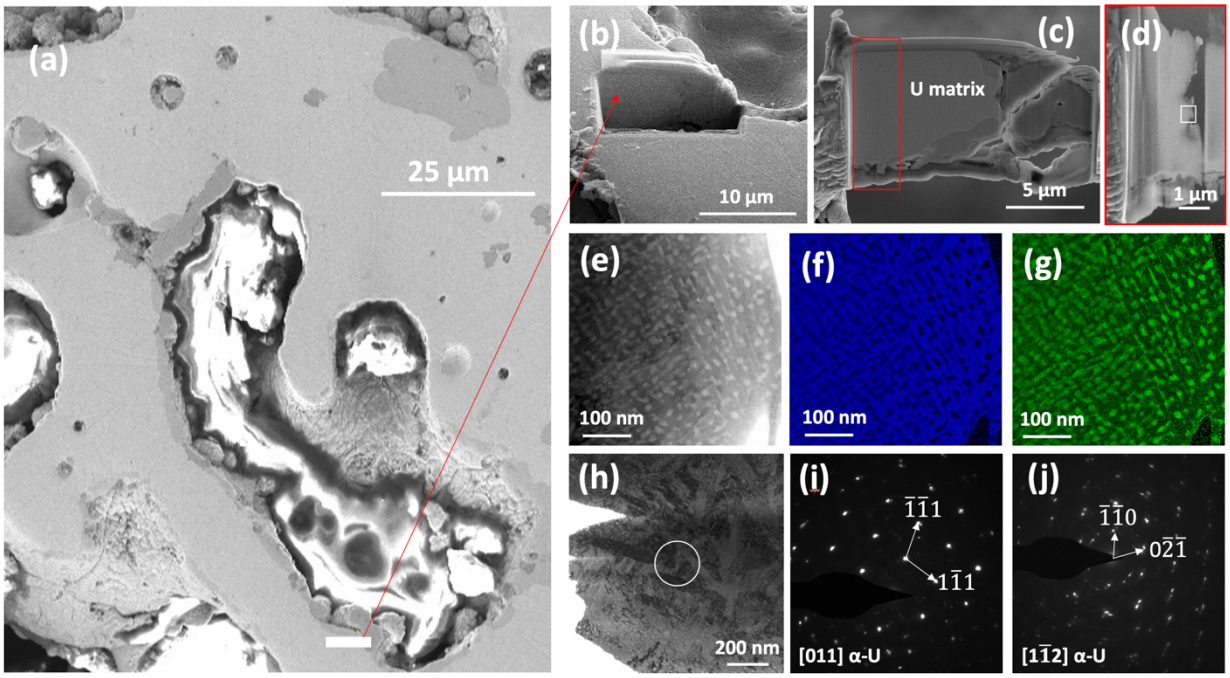

Figure 2. The location (a) where FIB-TEM sample was prepared (white band) has a pore as large as 100 µm and of irregular shape, indicating the pores are interconnected; (b-c, red box is d before thinning) showing the both U matrix and lanthanide were well preserved during sample preparation; STEM EDS mapping ((e) is BF image, (f) is U map, and (g) is Zr map) of the region boxed by the white square in (d) shows the formation of nano sized Zr precipitates in the U matrix in a pattern, indicating crystal orientation. TEM SAED pattern indexing ((i) and (j), measured in the white circle shown in (h)) shows the dominant phase is α-U.

The lamella shown in Figure 5 was lifted from the b site in Figure 2 to investigate Zr concentration and its phase information in the fuel away from fuel cladding interface. Figure 5 shows the precipitation of excessive Zr out from α-U matrix. This region is still inside fuel region with U the dominant element and α-U the primary phase based on the SAED pattern (Figure 5 i-j) which shows multiple satellite spots along the major reflections for α-U. STEM-EDS shows 20 nm Zr clusters forms arrays possibly following preferred crystal orientation of α-

198 U. The overall concentration of Zr in this region is close to 14 at.%, a value higher than those
199 found at fuel rim near fuel cladding interface. The elevated concentration indicates the
200 movement of Zr from the outer fuel region to the center, reconciling the known “Zr
201 redistribution”, which will be discussed in section 4.2. The darker region in sample c is identified
202 as lanthanides and the associated phases and will be reported in a separate paper.
203
204 3.3. Fuel inner radial region
205 SEM-EDS shows this region has a Zr concentration close to 60 at.%, indicating a significant
206 Zr enrichment compared with the starting composition of U-23 at.% Zr. This region is mainly a
207 single phase with sparse secondary particles and fission gas bubbles much smaller in size than
208 those observed in the outer radial region of the fuel shown in Figures 1 and 2. Two TEM lamella
209 have been prepared from this region. One is close to the fuel center (c in Figure 2) and the other
210 close to the boundary between the inner and outer fuel regions (d in Figure 2).
211
212 3.3.1. ω phase in γ matrix
213 This lamella was prepared from a site close to fuel center (c in Figure 2) and is shown in
214 Figure 6. The major phase is identified as bcc-UZr_{2+x} (here x can be either positive or negative,
215 depending on the actual chemical composition) with nano-sized omega (ω) phase embedded.
216 SAED patterns of these thin areas (g and j) displays two sets of patterns with the stronger set
217 (yellow colored circles) for the bcc matrix and the weaker set (white colored circles) for ω phase.
218 The weaker set for ω particles was replaced by streaked lines of intensity on the SAED patterns
219 (Figure 6k) for the thicker region, indicating the ω phase in the thicker region are an embryo
220 stage of omega phase [17]. Compared with the thin region, data from the thicker region is more
221 representative of this region since the weaker set of diffraction spots found in the thin region

could be due to ion irradiation during FIB sample preparation [18].

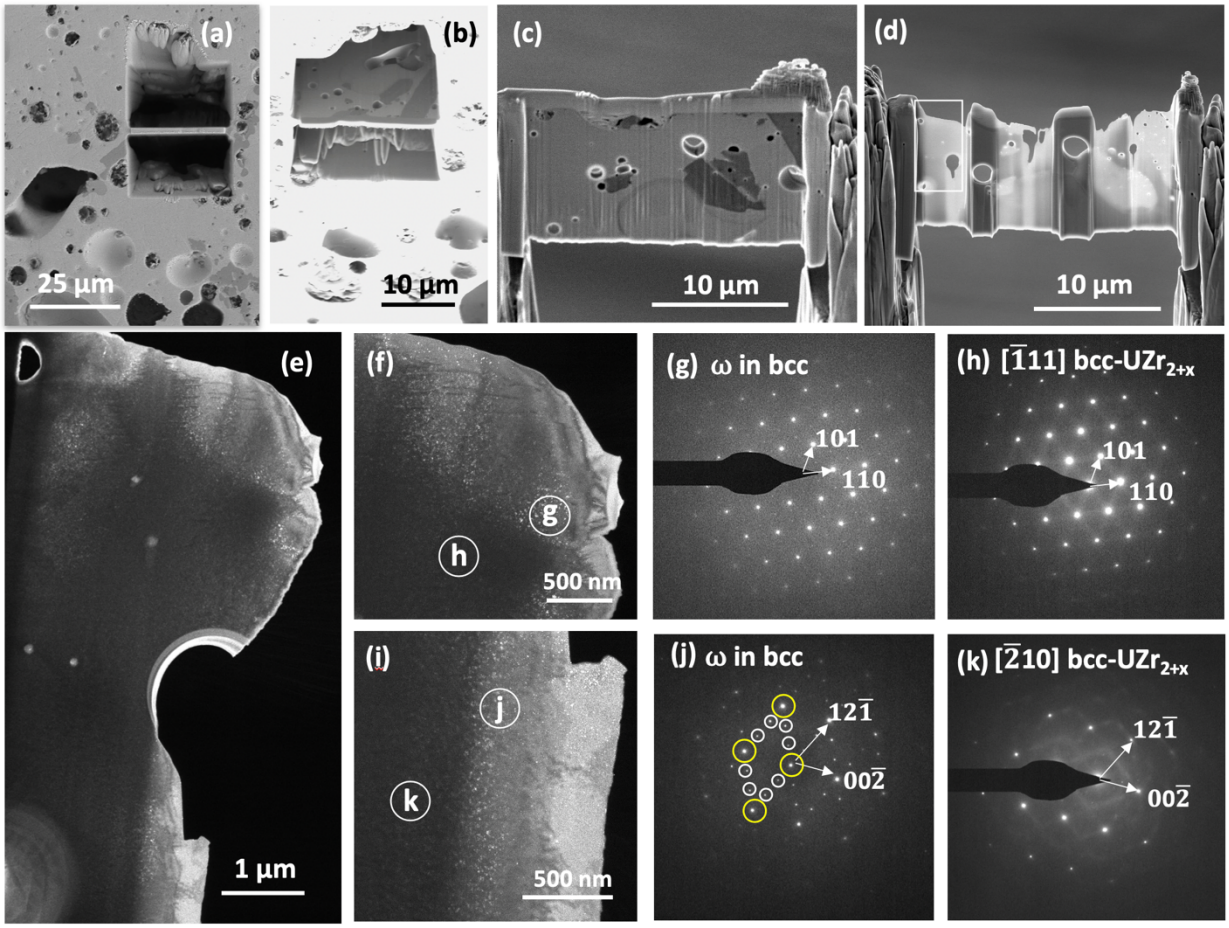

Figure 3. A FIB-TEM sample prepared in the center UZr_{2+x} region (a-d); There was sample loss during instrument loading. The lamella region shown in (e), from the area highlighted by the white box in (d), is the matrix with secondary phases as indicated by the white areas in the dark field image. This secondary phase is observed in the thinner regions, as highlighted in the magnified images shown in (f) and (i). TEM SAED patterns were colleted at points g, h, j, and k (shown in (f) and (i). The patterns taken from the thinner areas ((g) and (j)) indicate the bright phase is ω phase in a bcc γ phase matrix. Patterns from the thicker regions (h) and (k)) shows the replacement of distinctive spots for ω phase by diffused streaks for ω embryo, while spots for bcc matrix are preserved.

3.3.2. Spinodal decomposed γ matrix

This lamella was prepared from a site close to the boundary between outer and inner radial regions (d in Figure 2) and is shown in Figure 7. Figure 7a and b shows the location of the

lamella liftout and the lamella prepared from the single phase UZr_{2+x} region close to boundary between outer and inner radial region. SAED patterns indicate the region is also ω phase in a bcc matrix (Figure 7f). A series of BF images (7c through 7f) collected at gradual increasing magnifications of the region highlighted by the white box in 7b shows a microstructure of nanoscale domains throughout the entire fuel center region (the other areas besides the black region in Figure 7b are primarily lanthanide). STEM EDS data indicates the nanoscale domains are compositionally fluctuating. Those two pieces of evidence together point to a spinodal decomposed microstructure.

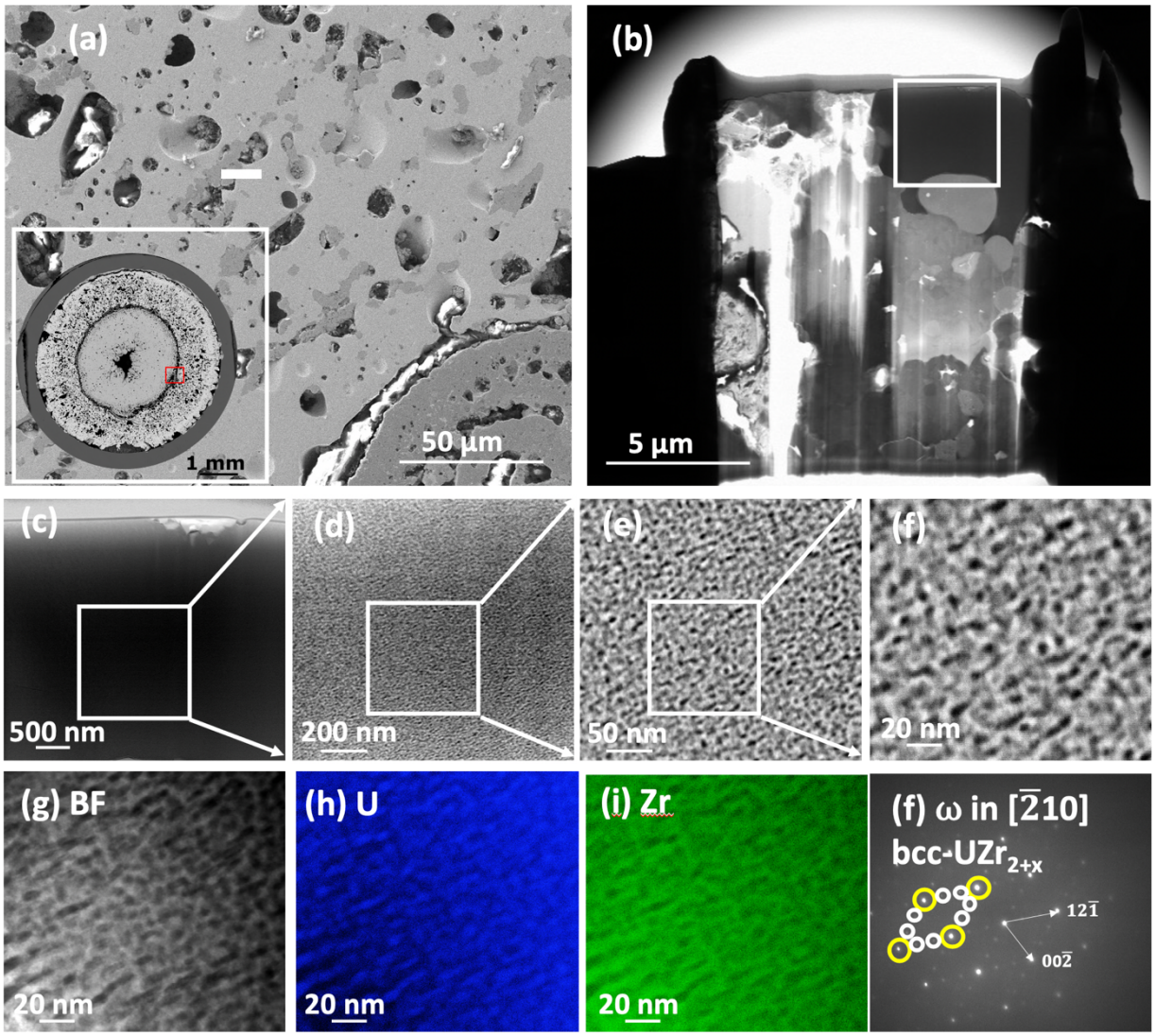

Figure 4. Characterization of FIB-TEM sample prepared inside UZr_{2+x} phase near casting interface. (a) shows the region highlighted by red box in the inset image. The lamella shown in (b) was lifted from the location indicated by the white line in (a). The magnified images ((c) through (f)) of the white box shown in (b) indicate this area is highly homogenous and contains nanosized domains. STEM-EDS mapping (g-i) shows those domains are a compositional fluctuation of U and Zr. The SAED pattern shown in (f) indicates the co-existence of ω phase with this decomposed bcc-UZr_{2+x} phase

3.4. Boundary between outer and inner radial region

The lamella shown in Figure 8 is labeled as e in Figure 2. The interface between the fuel outer and inner radial regions contains fragmented but intertwined rinds enriched by Zr and Si. Figure 8 shows the lamella and the detailed characterization of this rind. Figure 8c shows the

rind is polycrystalline with submicron sized grains. STEM EDS shows the distribution of U along the grain boundary of Zr_2Si (Figure 8d and 8e). Indexing of the TEM SAED patterns collected reveals the polycrystalline phase is Zr_2Si with a tetragonal crystal structure (space group *I*4/*mcm* with a = 6.58 Å and c = 5.37 Å).

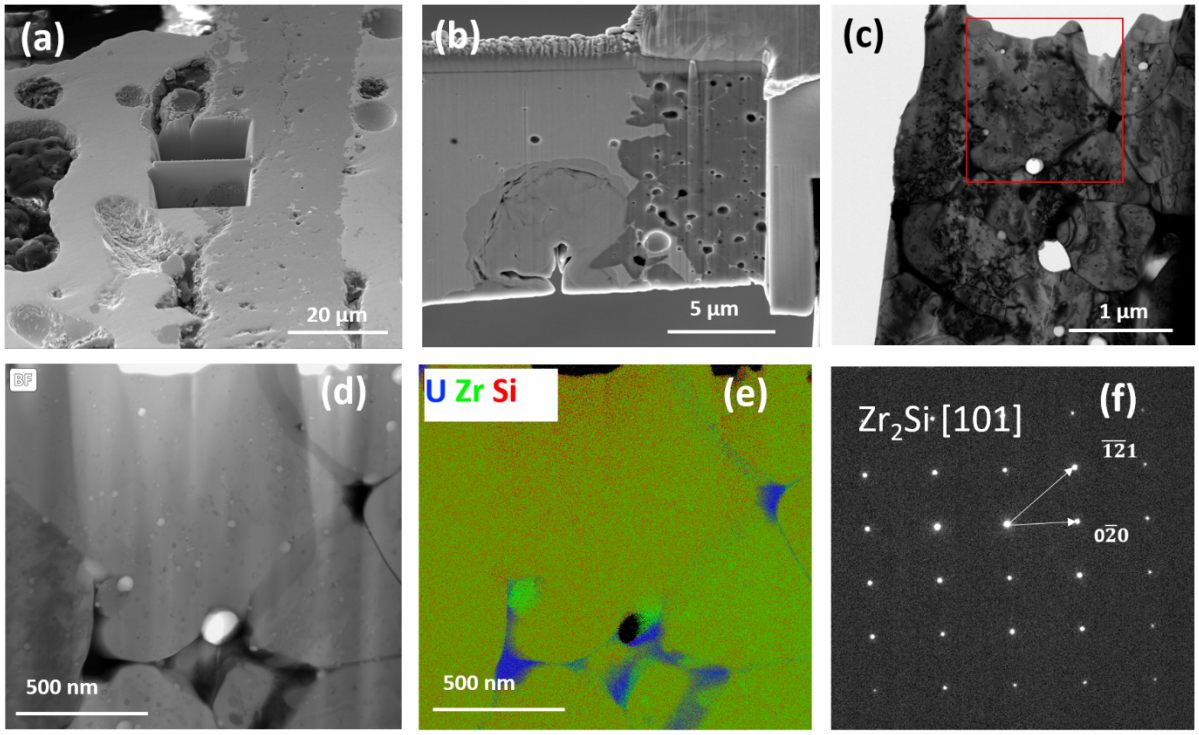

Figure 5. The FIB-TEM sample was prepared across the boundary between outer and inner radial fuel regions (a-b). The STEM-EDS (d) of the region highlighted in red box in (c) shows the major phase of the polycrystalline rinds is zirconium silicide with U located at grain boundaries (e). TEM SAED indexing (f) shows the boundary phase is Zr_2Si with a tetragonal crystal structure.

3.5. Formation of Zr rind

Formation of thin Zr rind was observed at two locations in the fuel. One is near the fuel-cladding interface and the other one at the fuel center. The two types of Zr rinds are formed through different mechanisms and are discussed separately in Sections 3.5.1 and 3.5.2.

3.5.1. Zr rind near fuel center

The lamella shown in Figure 9 was prepared at site f in Figure 2 near the fuel center. TEM characterization revealed a double-rind structure by STEM-EDS results, as shown in 9c. The major rind is Zr_2Si, and is the same phase/crystal structure as the boundary region shown in Figure 8 between the outer and inner radial fuel regions. The nearby Zr rich rind is of limited U and Si inside and crystallized as hexagonal α-Zr. STEM-EDS mapping shows multiple regions Zr rich particles inside Zr_2Si (Figure 9j), which could be the precursor for Zr rinds. The nearby UZr_{2+x} region (Figure 9m) is ω particles inside bcc-matrix.

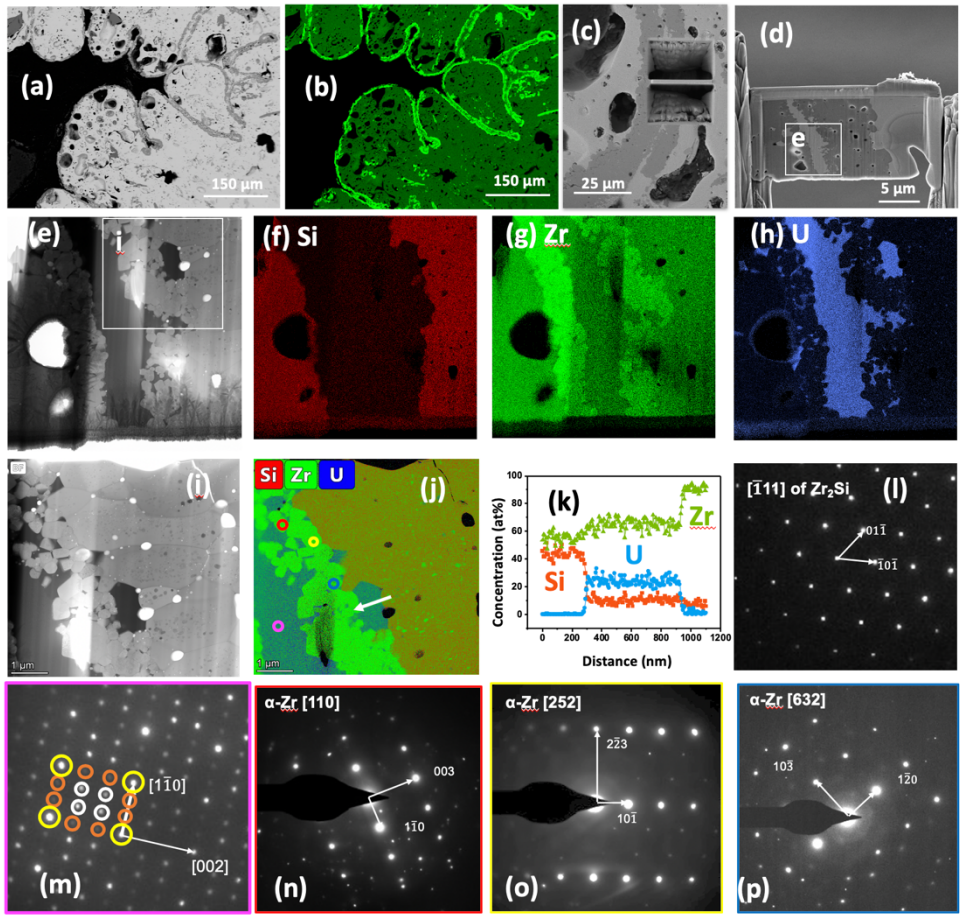

Figure 6. The region (a) where FIB-TEM sample is prepared points to a formation of rinds enriched by Zr (b) at the swelling frontier. The sample successfully captured the transient region between two rinds ((c)-(d)). STEM EDS mapping ((e) for BF image, (f) for Si, (g) for Zr, and (h) for U) shows the formation of a Zr dominated rind beside the major rind of zirconium silicide.

Higher magnification images ((i) and (j)) and a STEM EDS mapping overlay (j) with a line distribution of elements (k) starting in the Zr dominated region, crossing the UZr_{2+x} phase, and moving into the zirconium silicide rind indicates the Zr-rich rind is nearly pure Zr. SAED patterns show the major rind is Zr_2Si (l), UZr_{2+x} region is ω phase in a bcc matrix (white circles are for ω variants, orange circles are from double diffraction, while the yellow circles (strong spots) are for the bcc matrix (m). Different regions in the Zr-rich rind (colored circles in (j)) are indexed to be α-Zr ((n)-(p)).

3.5.2. Zr rind near fuel cladding interface

The lamella shown in Figure 10 is from site g in Figure 2, and is the characterization of the Zr rind formed at the fuel cladding interface. Small amounts of N and O were found in the Zr rind based on STEM EDS results. The most striking feature found is the crystal structure of this Zr rind as revealed by SAED patterns of three basic zone axis, shown in Figure 10h, i, and j. Instead of the stable hexagonal structure for the low temperature phase, or the bcc high temperature phase, it is a face centered cubic (fcc) structure with an estimated lattice parameter of 0.467 nm. This value is closer to fcc zirconium nitride (0.456 nm) than that for fcc Zirconium oxide (ZrO_2) (0.517 nm). The exact formation mechanism of this rind requires further investigation with out-of-pile separate effects studies.

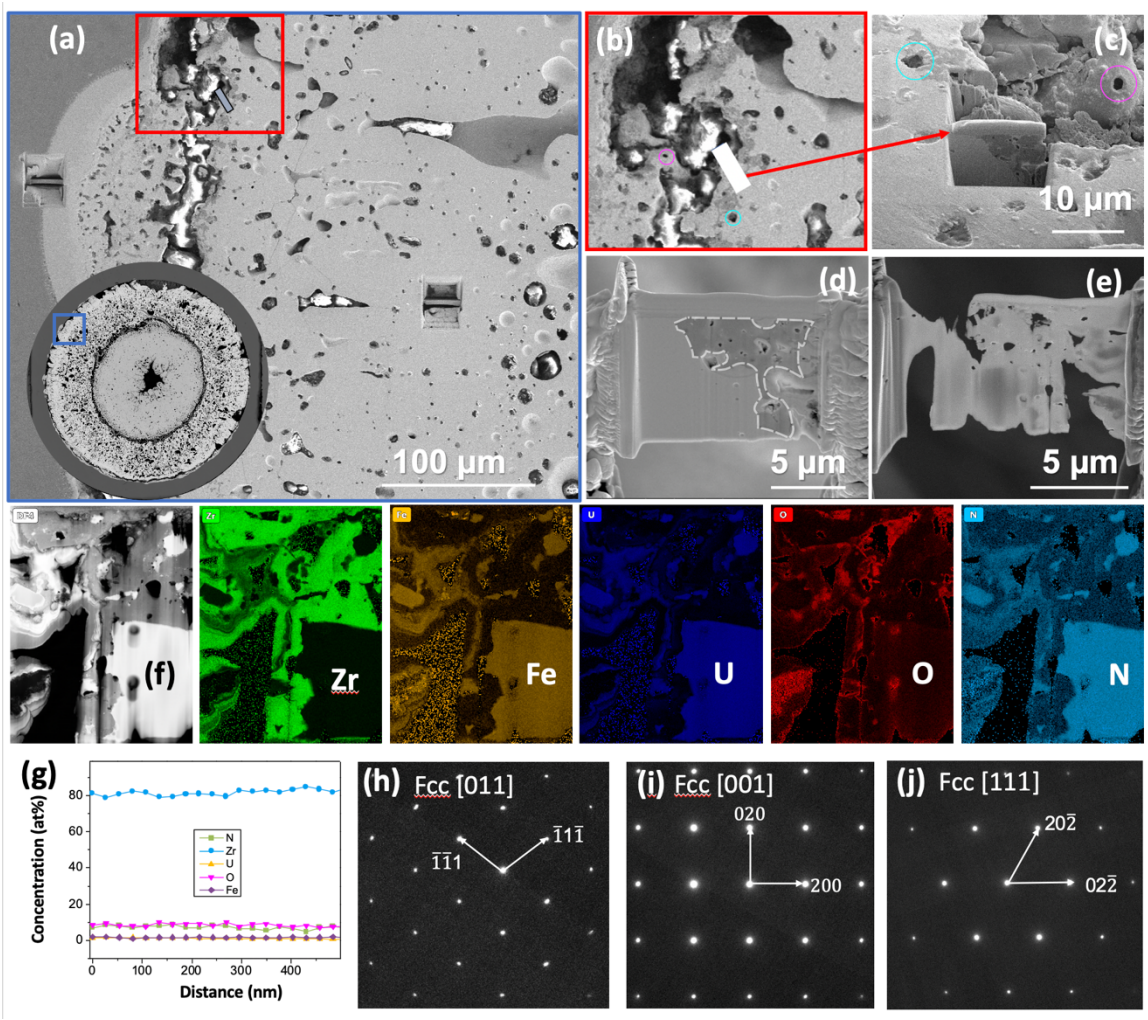

Figure 7. A FIB-TEM sample was prepared in the region highlighted by the red box in (a), in the location indicated by the blue box in the inset. The lamella location is shown in (c) with a blue rectangle, with other features highlighted by colored circles to cross reference the position. The region highlighted by a dashed line in (d) shows a porous structure. (e) STEM-EDS mapping ((f) for BF image followed by Zr, Fe, U, O, and N mapping) indicates the region outlined by the dashed line in (d) is enriched by Zr. Quantification (g) of STEM-EDS data shows the Zr enriched region also has N and O detected. TEM SAED patterns show this Zr-rich phase has a face centered cubic (fcc) crystal structure.

4. Discussion

4.1. Fuel swelling

Historically, the burnup limit of metallic fuel was raised to 20% by various innovative fuel pin designs and proven through EBR II and Fast Flux Test Facility (FFTF) irradiations. New development, led by INL under the support of AFC since 2000's, targets an ultrahigh burnup of

30% FIMA. Among the proposed strategy, annular fuel without a sodium bond was suggested to provide additional benefits that facilitate a direct geological disposal for waste handling. A long term strategy is to prepare annular U-10Zr based metallic fuel through a co-extruding route with cladding to drastically reduce process waste, eliminate the sodium bond, and reduce fuel fabrication cost to improve overall metal fuel economics [19].

During in-pile irradiation, metallic fuel swells rapidly in the first ~3% burnup due to the formation of isolated fission gas bubbles. The swelled fuel strains cladding from fuel cladding mechanical interactions (FCMI). For example, up to a 40% volume swelling was observed in Mark II U-5Fs fuels irradiated to first 2-3 % burnup [20]. The contribution from solid fission products is minimal as determined by extrapolation swelling curves from higher burnup regimes. This rapid swelling was significantly slowed when burnup reached 3% and the fission gas bubbles became interconnected, allowing rapid fission gas release into the plenum. After interconnected porosity develops, the solid fission products become the major source of fuel swelling, although with a significantly reduced swelling rate, and the associated FCMI becomes negligible. Historically, this problem was solved through decreasing fuel smear density to 75%, creating a wide fuel-cladding gap to accommodate radial expansion of the fuel from the initial rapid fuel swelling. By the time fuel and cladding contacted, the fission gas bubbles are large enough to be interconnected which leads to subsequent rapid dissipation of fission gas without significantly swelling the fuel.

To support the ultra-high burnup beyond 20% FIMA, the fuel smear density was further decreased to 55% and an annular design was adapted. In an annular fuel design, the fuel is put in close contact with the cladding at the beginning of irradiation. As fission gas initiates swelling in the fuel, high strength cladding, HT-9 in this case, prevents outward swelling of the fuel and forces the swelling inward towards the central annulus. Swelling into the annulus then prevents

348 the FCMI often observed in early metallic fuel irradiation [1, 3, 21]. Previous PIE data shows
349 that the fuel does indeed start to swell inwards under irradiation to fill the annulus [8, 9]. The PIE
350 data presented in this study, through extensive microstructure characterization and phase
351 identification, reveals that the spongy fuel annular region is single phase α-U with large fission
352 gas bubbles interconnected and a fuel center region of UZr_{2+x} with a moving front showing
353 curvatures that indicates an ongoing inward swelling behavior. In this fuel, inward swelling
354 progressed until the central annulus was nearly closed. At this burnup, swelling is mitigated since
355 80-90% of the fission gas is released and solid fission products are not yet a significant
356 proportion of the inventory. The fission gas release for this fuel pin was 77 % when nitrogen and
357 oxygen components of the sample from AFC-3A R4 are ignored [8].
358 This microstructural characterization provides further understanding regarding the
359 conclusions reported in Harp et al. [8] for the challenges in removing the Na bond in metallic
360 fuel. Specifically, the removal of the Na bond necessitates more stringent dimensional
361 specification for fuel slugs to prevent the fuel-cladding interaction observed in this
362 characterization. The infiltration of iron into this fuel is quite significant for this burnup (3.3%
363 FIMA) and the simulated linear heat generation rate. The 13 at.% Fe observed near the cladding,
364 shown in Figure 3, and the formation of U_6Fe discussed in Section 3.2.1 and shown in Figure 4
365 illustrate that local hot spots in the fuel can have a deleterious impact on fuel stability and
366 cladding integrity when the fuel slug is loosely coupled to the cladding. The solution to this issue
367 is to ensure tight machining tolerances on fuel cladding, as was achieved in later irradiation tests
368 of annular U-Zr fuel where there was no fuel-cladding interaction [9].
369
370 4.2. Zr Rind

371 The outermost layer in the fuel is enriched by Zr and was identified as single phase with over
372 80 at.% Zr, with the balance being O and N (Figure 10 g), hereafter being referred to as "Zr
373 rind". The formation of Zr rind was reported for irradiated EBR II and FFTF U-Pu-Zr fuel pins
374 [22] as well as out-of-pile diffusion couple studies [23]. Casting samples with ZrO_2 wash to
375 facilitate pin removal from the quartz can also foster the formation of Zr rind. Considering this
376 sample has also been cast in quartz with a ZrO_2 wash [24], the formation mechanism of Zr rind
377 observed here cannot be exclusively attributed to any one of the abovementioned factors.
378 Although its formation mechanism is still under debate, the Zr rind has been observed to be
379 an effective diffusion barrier to mitigate FCCI. Due to this, the integrity of the rind is important,
380 especially at medium to high burnup when FCCI becomes one of the key factors that limits the
381 fuel life. A previous study shows an intact Zr rind observed at a burnup of 2.5 at.% can break
382 apart into large Zr particles at a higher burnup of 7% [25]. Since the crystal structure is one of
383 the factors affecting the mechanical response of the Zr rind, it is necessary to determine its
384 crystal nature. Unfortunately, this information was not previously investigated, and it was
385 generally assumed to be impurity (primarily O and N) stabilized α-Zr.
386 The current study shows the Zr rind is of fcc crystal structure, instead of the low temperature
387 hexagonal α-Zr or the high temperature bcc β-Zr. The formation of fcc-Zr rind in this irradiated
388 fuel may be related to irradiation or microstrain [26], although the role played by O and N
389 impurity cannot be ruled out. A similar fcc-Zr was also found in a fresh U-Pu-Am-Np-Zr
390 metallic fuel for minor actinide destruction [27], raised a concern over the credibility to simply
391 treat Zr precipitates as α-Zr in U-Zr based nuclear fuel. The estimated lattice parameter indicates
392 the crystal structure of the Zr rind is closer to ZrN, although the role played by oxygen cannot be
393 ruled out. The oxygen and nitrogen impurities were likely introduced during fuel fabrication.
394 4.3. Zr redistribution

For U-Zr based metallic fuel, Zr redistribution is widely reported in PIE observations of irradiated fuel [28, 29, 30, 31]. The driving force can be a combination of temperature gradient, elemental concentration gradients, irradiation effects, and phase transformations depending on fuel burnup. In U-10Zr fuel zones, restructuring is observed that can be correlated to chemical stability and mobility of Zr at different temperatures in the different U-Zr phases that are present across the temperature gradient present under irradiation. Zirconium is not miscible in the α or β phase of U but is fully miscible in the γ phase. Zirconium is of low mobility in α-U, but is highly mobile in β-U [29]. Thus Zr at the periphery of the fuel that is below the α/β U phase transition temperature tends to not migrate in the fuel, while Zr in the region of the fuel in the β-U phase migrates up the temperature gradient to the central region of the fuel that is in the γ-U phase [28]. The temperature of these phase transitions under irradiation is also not clear and may be shifted due to the dynamic conditions of irradiation in contrast to the steady state conditions reported in phase diagrams [22].

In this sample, Zr redistribution has occurred to an extreme amount not seen in sodium bonded U-10Zr. After cooling from irradiation, the zone with Zr depletion is revealed to be predominantly singe phase α-U, except for the formation of U_6Fe near cladding region. Samples lifted from the outer fuel region, between the fuel-cladding interface and the central region are revealing several interesting results.

In the fuel region at the fuel-cladding interface, a diffusion zone was identified between the fuel and cladding as shown by the infiltration of Fe along certain crystallographic paths of α-U (see Figure 4). The grains have columnar shapes elongated roughly along the direction of Fe penetration from cladding into fuel in a depth of 200 μm. Additionally, there is no Cr infiltration into the fuel which follows the fuel-cladding interaction behavior observed previously in HT-9 clad metallic fuels [16, 31]. Beyond this region into the fuel, there is an increase of Zr

concentration with the disappear of Fe (Figure 3).

At the region close to two region boundaries, site b in Figure 2, the microstructure shows a α-U with nano sized Zr clusters embedded inside the grains (see Figure 5). The overall Zr concentration in this region is 28.4% based on STEM EDS data, indicating α-U alloy is in a supersaturated condition before the formation of Zr clusters. An explanation for this may due to the high temperature γ phase since this region is closer to fuel center. The γ phase has much higher solubility limit of Zr inside U. During cooling, U went through the phase change from γ- to α-phase with much lower solubility of Zr, resulting in nano-sized precipitates of Zr as previously observed [32].

The center region is single phase UZr_{2+x} with a microstructure of omega precipitates embedded in a decomposed bcc matrix. The formation mechanism and phase transformation of this region is linked to the temperature profile along the radial direction. Detailed phase analysis points to a temperature profile that follows the general trends of a parabolic decrease from UZr_{2+x} center region to UZr_{2+x} outer region with a center temperature higher than 610 ℃ and outer region below cooler than this. Indeed, the center line temperature was estimated to be ~900 °C.

On the U-Zr system phase diagram [11], UZr_{2+x} is the only intermetallic compound with a hexagonal crystal structure at room temperature. Above ~610 ℃, it becomes γ-(U,Zr), a solid solution of bcc crystal structure. During cooling, the phase change from bcc to hexagonal follows the "ω phase transformation", leading to the formation of ω phase, a metastable phase that will transform to hexagonal δ-phase upon subsequent annealing. Extended annealing can be required to fully order the ω phase to δ phase. The appearance of ω nano particles in the bcc matrix (Figure 6f and i) indicates this part of fuel was in the γ-(U,Zr) phase during irradiation. During cooling, the ω phase starts to form in the bcc matrix, but stopped at a lower level of ordering,

possibly due to insufficient time at high temperature.

At the outer edge of the UZr_{2+x} center region, the microstructure was found to have a nanoscale composition fluctuating (see Figure 7d – f), due to spinodal decomposition. The SAED also shows the same pattern (Figure 7f) as the UZr_{2+x} center region (Figure 6j), but with no omega phase being clearly observed. The reason can be attributed to the lower temperature in this region during irradiation. This region remained as ω phase during the entire life in reactor because the temperature was below 610 °C. Neutron irradiation, however, enhanced element diffusion and triggered spinodal decomposition at this lower temperature in a similar mechanism as observed for ω phase irradiated by heavy ion [33].

4.4. Fission gas bubbles and pores

The formation of fission gas bubbles in irradiated nuclear fuel is directly related to the low solubility of inert fission gas atoms, such as Kr and Xe, inside the fuel matrix. For U-10Zr metallic fuel [34], right after being generated by fission reaction, fission gas atoms cluster along preferential sites either along high angle grain boundaries of α-U or the phase boundary between α-U and δ-UZr_2, forming nano sized fission gas bubbles. As the irradiation continues, the surrounding fuel matrix continues to feed the gas bubble with fission gas atoms and vacancies generated by irradiation damage to support the growth of gas bubbles into micron sized pores. Therefore, the formation and growth of fission gas bubbles into large pores is dictated by the diffusion of fission gas atoms, vacancies, and interstitials, through the fuel matrix.

Strikingly different size and distribution of fission gas bubbles and pores are found between the α-U region and the UZr_{2+x} center region in this annular fuel pin. The majority of the α-U region, except for close to the fuel-cladding interface, shows large pores interconnected to a size close to 200 μm. In contrast, the pores in the center UZr_{2+x} region are substantially smaller at ~ 10 μm separated from each other by ~20 μm in a matrix of UZr_{2+x} of ~5 nm spinodal

decomposed domains.

Although the different fission density could also be a potential factor, it alone cannot account for the roughly 20 times difference in pore size. Fuel temperature prediction based on the BISON model [35] shows the fuel centerline temperature was near 900 ℃ (UZr_{2+x} region) and drops to ~700 ℃ in the U region. The fission gas bubbles in the U region, however, are 20 times larger than in UZr_{2+x} region. Although other factors, such as strains can play the role in the fission gas bubble size, the primarily possible reason, however, can be attributed to the different amount of phase boundary area, which can act as an effective sink for vacancy and interstitial recombination loss, cutting the supply of vacancies for bubble growth in metallic fuel [34]. Although the grain size of α-U was not determined in the current study, it is safe to assume the size is much larger than a TEM lamella size. The UZr_{2+x} microstructure is shown in Figure 7 at room temperature and is expected to have a spinodal decomposed microstructure with a domain size of ~5 nm at an elevated irradiation temperature. These domains share elastic semi-coherent boundaries that provides a large amount of interface to annihilate vacancies and impede gas bubbles growth in the UZr_{2+x} region. These factors may be the primary causes of different pore size and distribution found in the α-U and UZr_{2+x} phases although the two phases are irradiated side-by-side by neutron.

4.5. Irradiation behavior of U and UZr_{2+x}

The irradiation damage response of metallic fuels is quite different from ceramic fuels. While the irradiation behavior of ceramic fuel is mainly composed of the generation of point defects, the movement of microscopic pores and microstructure reconstruction, the irradiation behavior of metallic fuel is directly focused on the generation of microscopic and mesoscopic pores and fission product movement through those pores. Although the irradiation of U-10Zr has been well studied in the past, there is no separate study for the two major phases, i.e., the single-phase U

and UZr_{2+x} phase.

The irradiation induced effects in single phase U progressed with radiation dose quickly into a regime dominated by growth of fission gas bubbles and formation of voids, possibly due to the low melting point and mechanical softness not allowing U to resist the growth of pressurized bubbles. The initiation and growth of gas bubbles inside α-U irradiated by 140 KeV Helium (He) beam [36] at ambient temperature reveals the formation of large spherical bubbles up to 70 nm at an ion fluence of 5×10^{16} ions/cm^2 (5 dpa), and the bubble size reached the upper limit allowed for TEM analysis due to the sample thickness limitation. In the literature, the irradiation defects in U at the very early stage of irradiation remains unexplored, except for one study [37] showing the type of dislocation loops in α-U formed by neutron irradiation. Apparently, the early stage of defect evolution in α-U is not as important as those for irradiation induced bubbles, since the latter plays a larger role on the physical property evolution with irradiation, such as swelling and thermal behaviors, of single phase U.

Likewise, there are relatively fewer reports on the irradiation of the UZr_{2+x} phase. Because it is an intermetallic compound, some of the irradiation induced effects, such as disorder and amorphization [38, 39], that are commonly observed for uranium-based intermetallics are expected to take place in irradiated UZr_{2+x}. Surprisingly, they do not occur. A recent in-situ TEM observation [33] of ion irradiation of UZr_{2+x} shows a compositional fluctuation between domains with a wavelength of 20 to 40 nm at a radiation dose as low as 0.2 dpa, suggesting a spinodal-like phase decomposition. The current study also reveals a similar microstructure with domain sizes ranging from 5 to 10 nms. The size difference could be from the different irradiation dose and dose rate between ion and neutron irradiation. However, the similarities of the microstructure in the UZr_{2+x} region between those two irradiation conditions suggests that certain neutron irradiation effects can be well replicated by ion irradiation, although the difference of

dose rate needs to be considered when extrapolating the results of ion irradiation to neutron irradiation. Furthermore, the ion irradiation temperature can be well controlled, whereas the fuel temperature varies along the fuel radial direction. Such disparity, however, can be well justified by economic factors, such as much shorter time and lower cost for ion irradiation, when a quick screening of candidate materials is highly desirable for next generation nuclear reactors.

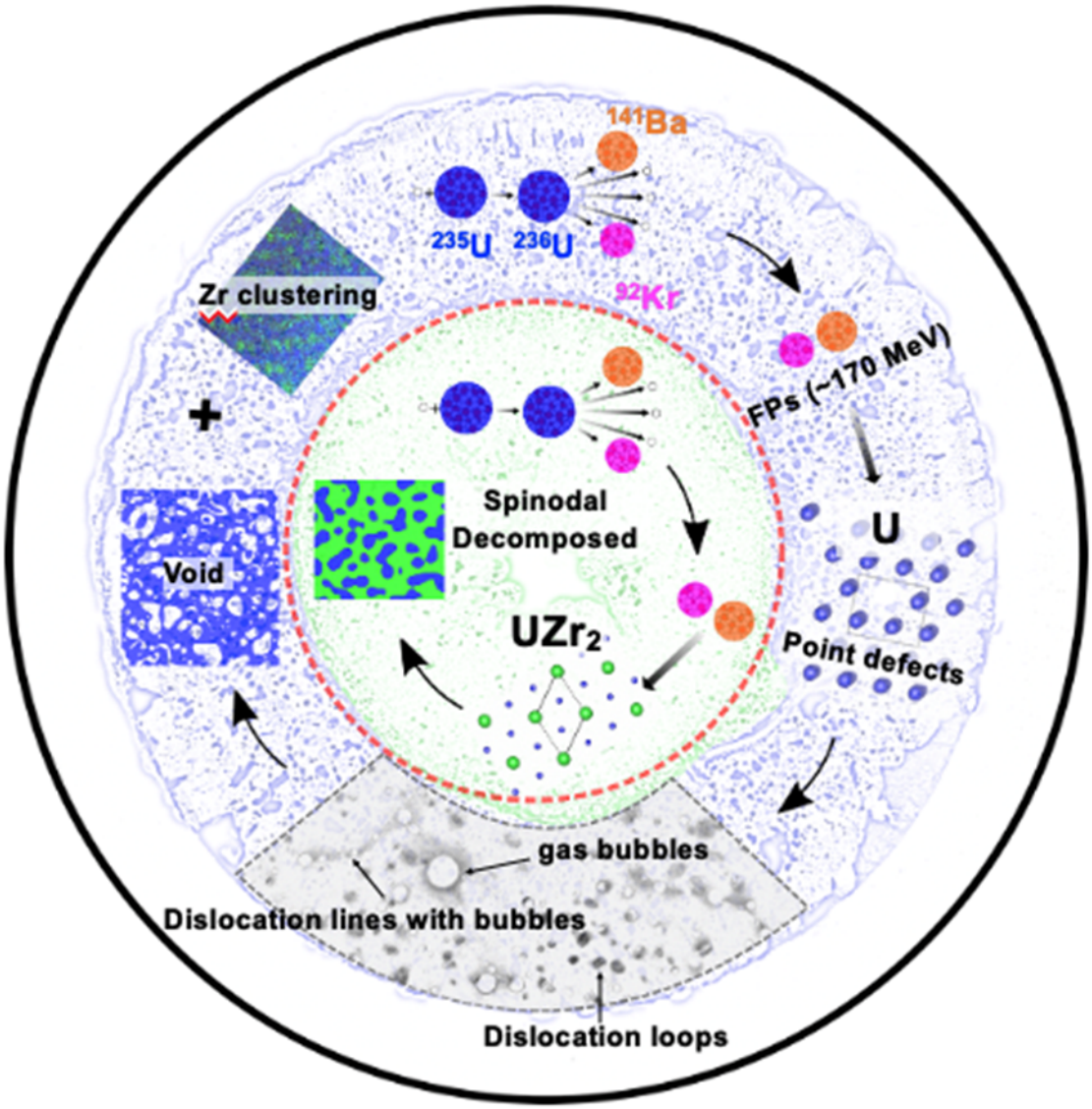

Figure 11. The scheme of irradiation behavior for α-U and ω-UZr_{2+x} with the neutron irradiated annular fuel overlaid, showing the different dominant microstructures inside the center and annular regions and their formation mechanisms.

The current study provides a chance to explore the different irradiation behavior of α-U and ω-UZr_2 separately, as shown in Figure 11. The inner and outer radial regions are mainly ω-UZr_2 and α-U, respectively. Substantially different irradiation behaviors between the two phases are highlighted by the evolution path, started with nuclear fission reactions. In α-U, there may be the generation of point defects and following growth into extended dislocation loops and lines, but its irradiation behavior is more dominated by the formation and growth of fission gas bubbles into voids and pores. The α-U may have clusters of Zr or form U_6Fe intermetallic nano particles depending on the presented "foreign" elements. On the contrary, a radiation induced spinodal decomposed microstructure dominates the irradiation behavior of UZr_{2+x}. An in-situ TEM study shows the spinodal decomposed microstructure can be formed by heavy ion irradiation for 0.2 dpa at 550 ℃ [40]. The domain size after heavy ion irradiation is ~20 nm, in contrast to ~5 nm after neutron irradiation (Figure 7). BISON modeling [35] indicates the temperature at this region is ~800 ℃ during neutron irradiation. A higher irradiation temperature but smaller domain size suggests that other factors, such as cascade size and irradiation induced mixing effects, might play a role in spinodal decomposition of UZr_{2+x} phase. The evolution of this spinodal decomposed microstructure with higher irradiation dose and its effect on the fission gas bubble formation and growth remains unexplored and worthy of further studies.

A side-by-side comparison (Figure 12) of the irradiated microstructure between UZr_{2+x} and Zr_2Si, two Zr-based intermetallics, clearly reveals the different irradiation behaviors under similar neutron irradiation temperatures, regardless of slightly different dpa values (Figure 12). The Zr_2Si grain bears similar features of single crystal crystalline materials being irradiated by showing the formation of irradiation defects, such as dislocation loops, lines, and gas bubbles. However, none of these features are observed in the neighboring UZr_{2+x}, except for the spinodal decomposed microstructure. The reason can be attributed to the phase instability of the two

phases. The spinodal decomposition of the UZr_2 phase can be partially attributed to the phase change from hexagonal to bcc at 610 ℃, while the Zr_2Si phase is stable up to 1925 ℃.

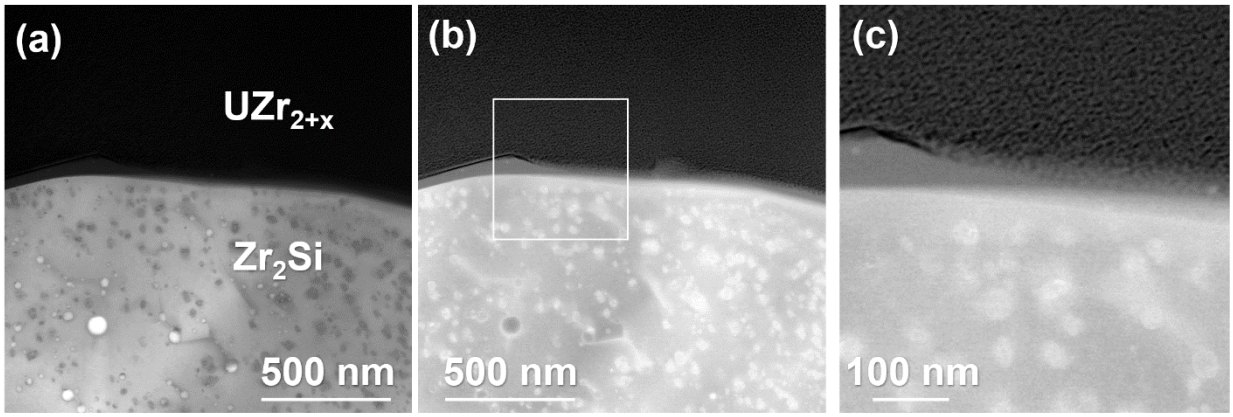

Figure 12. Microstructure of UZr_{2+x} and Zr_2Si showing different irradiation behavior of the two phases. (a-b) is the STEM BF and DF images of a two-phase region. (c) is a magnified image of boxed region in (b) showing the UZr_{2+x} is dominated by spinodal decomposed nano domains while Zr_2Si is featured by radiation induced dislocation loops.

5. Conclusion

The current study provides an advanced microscopy-based multiple scale characterization of neutron irradiated annular U-10Zr, focusing on the neutron irradiation effects in the two prominent phases of the U-Zr system: α-U and ω-UZr_2. The results provide novel insight and understanding of the neutron irradiation behavior for U-Zr based nuclear fuel at a resolution down to nanoscale with following results:

- α-U was identified as the primary phase in the U dominant region.
- The fuel-cladding interface has Fe infiltration that preeminently changed the α-U grain size and shape, as well as fission gas bubbles regarding their size and distribution.
- In a region with higher Zr concentration, nano Zr clusters were observed and tentatively attributed to precipitation of Zr from a supersaturated high temperature γ-

phase during cooling after irradiation.

- ω-UZr_{2+x} near the fuel center contains nano ω variants in the bcc matrix, showing the typical microstructure of ω-UZr_{2+x} quenched from the bcc temperature region (above 610 ℃) based on an out-of-pile separate effects study.
- ω-UZr_{2+x} near the UZr_{2+x} and U phase boundary shows no ω variants but a spinodal decomposed microstructure with U and Zr composition fluctuation, indicating this region of ω-UZr_{2+x} was kept under the phase change temperature of 610 ℃.
- The two-phase boundaries are primarily composed of polycrystalline Zr_2Si in a tetragonal crystal structure with U occupying the intergranular spaces.
- A Zr-rich rind formed on top of Zr_2Si, likely the result of irradiation-induced formation of Zr cluster in Zr_2Si.
- The Zr rind formed at the fuel-cladding interface has an fcc crystal structure, potentially due to O and N impurities.

The U-10Zr annular fuel accommodated dramatic swelling by an inward swelling mechanism with little fuel cladding strain. At a burnup of 3.3%, the fuel center is still open with more space to accommodate additional fuel swelling due to solid fission products, while the α-U region is highly porous with interconnected pores. Both factors indicate additional swelling behavior of the fuel will be similar to solid metallic fuel. Therefore, this fuel demonstrates the potential of replacing a sodium bonded solid fuel with a helium bonded annular fuel design.

Acknowledgment

This work was financially supported by the Center for Thermal Energy Transport under Irradiation, an Energy Frontier Research Center funded by the Office of Science, Basic Energy

Sciences. This research used resources of the Irradiated Materials Characterization Laboratory, which is supported by U.S. Department of Energy, Office of Nuclear Energy under DOE Idaho Operations Office Contract DE-AC07-051D14517. This manuscript has been authored in part by UT-Battelle, LLC under Contract No. DE-AC05-00OR22725 with the U.S. Department of Energy. The United States Government retains and the publisher, by accepting the article for publication, acknowledges that the United States Government retains a non-exclusive, paid-up, irrevocable, world-wide license to publish or reproduce the published form of this manuscript, or allow others to do so, for United States Government purposes. The Department of Energy will provide public access to these results of federally sponsored research in accordance with the DOE Public Access Plan (http://energy.gov/downloads/doe-public-access-plan).

References

[1] G.L. Hofman, L.C. Walters, T.H. Bauer, Metallic fast reactor fuels, Progress in Nuclear Energy 31(1) (1997) 83-110.

[2] S. Hayes, D. Dempsey, J.M. Harp, G.L. Povirk, Developmental Objectives for Advanced Reactor Fuels, Idaho National Lab.(INL), Idaho Falls, ID (United States), 2017.

[3] L. Blake, Achieving high burn-up in fast reactors, Journal of Nuclear Energy. Parts A/B. Reactor Science and Technology 14(1-4) (1961) 31-48.

[4] D.C. Crawford, D.L. Porter, S.L. Hayes, Fuels for sodium-cooled fast reactors: US perspective, Journal of Nuclear Materials 371(1) (2007) 202-231.

[5] L.L. Briggs, Y.I. Chang, Safety Analysis and Technical Basis for Establing an Interim Burnup Limit for Mark-V and Mark-VA Fuel Subassemblies in EBR-II, Argonne National Lab.(ANL), Argonne, IL (United States), 2018.

[6] W. Carmack, S. Hayes, J. Harp, R. Fielding, S. Maloy, T. Saleh, Overview of the US DOE fast reactor fuel development program, Idaho National Lab.(INL), Idaho Falls, ID (United States), 2017.

[7] M.F. Simpson, P. Sachdev, Development of electrorefiner waste salt disposal process for the EBR-II spent fuel treatment project, Nuclear Engineering and Technology 40(3) (2008) 175-182.

[8] J.M. Harp, H.J.M. Chichester, L. Capriotti, Postirradiation examination results of several metallic fuel alloys and forms from low burnup AFC irradiations, Journal of Nuclear Materials 509 (2018) 377-391.

[9] J.M. Harp, L. Capriotti, F. Cappia, Baseline Postirradiation Examination of the AFC-3C, AFC-3D, and AFC-4A Experiments, Idaho National Lab.(INL), Idaho Falls, ID (United States), 2018.

[10] A. Aitkaliyeva, J. Madden, B. Miller, J. Cole, Implementation of focused ion beam (FIB) system in characterization of nuclear fuels and materials, Micron 67 (2014) 65-73.

[11] R. Sheldon, D. Peterson, The U-Zr (uranium-zirconium) system, Bulletin of Alloy Phase Diagrams 10(2) (1989) 165-171.

[12] S. Irukuvarghula, S. Ahn, S.M. McDeavitt, Decomposition of the γ phase in as-cast and quenched U–Zr alloys, Journal of Nuclear Materials 473 (2016) 206-217.

[13] S. Ahn, S. Irukuvarghula, S.M. McDeavitt, Thermophysical investigations of the uranium–zirconium alloy system, Journal of Alloys and Compounds 611 (2014) 355-362.

[14] S. Hayes, J. Harp, H. Chichester, R. Fielding, R. Mariani, W. Carmack, Advances in Metallic Fuels for High Burnup and Actinide Transmutation, Idaho National Lab.(INL), Idaho Falls, ID (United States), 2016.

[15] R. Fielding, P. Hansen, T. Hyde, J. Maupin, Fabrication Report for the FY11 Phases of the AFC-3A and 3B Irradiation Experiments, Idaho National Laboratory Report, INL/LTD-11-23158 (2011).

[16] D.D. Keiser, 3.15 - Metal Fuel-Cladding Interaction, in: R.J.M. Konings (Ed.), Comprehensive Nuclear Materials, Elsevier, Oxford, 2012, pp. 423-441.

[17] T. Li, D. Kent, G. Sha, L.T. Stephenson, A.V. Ceguerra, S.P. Ringer, M.S. Dargusch, J.M. Cairney, New insights into the phase transformations to isothermal ω and ω-assisted α in near β-Ti alloys, Acta Materialia 106 (2016) 353-366.

[18] K. Nuttall, D. Faulkner, The effect of irradiation on the stability of precipitates in Zr-2.5 WT% Nb alloys, Journal of Nuclear Materials 67(1-2) (1977) 131-139.

[19] A. Wright, S. Hayes, T. Bauer, H. Chichester, G. Hofman, J. Kennedy, T. Kim, Y. Kim, R. Mariani, W. Pointer, Development of Advanced Ultra-High Burnup SFR Metallic Fuel Concept- Project Overview, Transactions of the American Nuclear Society 106 (2012) 1102-1105.

[20] G. Hofman, Irradiation behavior of experimental Mark-II Experimental Breeder Reactor II driver fuel, Nuclear Technology 47(1) (1980) 7-22.

[21] J.H. Kittel, B.R.T. Frost, J.P. Mustelier, K.Q. Bagley, G.C. Crittenden, J. Van Dievoet, History of fast reactor fuel development, Journal of Nuclear Materials 204 (1993) 1-13.

[22] C. Matthews, C. Unal, J. Galloway, D.D. Keiser, S.L. Hayes, Fuel-Cladding Chemical Interaction in U-Pu-Zr Metallic Fuels: A Critical Review, Nuclear Technology 198(3) (2017) 231-259.

[23] W. Zhuo, Y. Xie, M.T. Benson, Q. Yang, R.D. Mariani, J. Zhang, Experimental Investigation of FCCI Using Diffusion Couple Test Between UZr Fuel with Sb Additive and Cladding, Nuclear Science and Engineering (2020) 1-15.

[24] C.A.P. T.P. O'Holleran, L.N. Squires, T.A. Hyde, J.R. Kennedy, T. Hartmann, AFC-3 Fuel

Characterization, Idaho Natl. Lab. Rep. (2012) INL/LTD-12-24346.
[25] S. Brémier, K. Inagaki, L. Capriotti, P. Poeml, T. Ogata, H. Ohta, V.V. Rondinella, Electron probe microanalysis of a METAPHIX UPuZr metallic alloy fuel irradiated to 7.0 at.% burn-up, Journal of Nuclear Materials 480 (2016) 109-119.
[26] C. Hitzenberger, H.P. Karnthaler, A. Korner, In situ tem study of the h.c.p. to f.c.c. martensitic phase transformation in CoNi single crystals, Acta Metallurgica 36(10) (1988) 2719-2728.
[27] D.E. Janney, J.R. Kennedy, J.W. Madden, T.P. O'Holleran, Crystal structure of high-Zr inclusions in an alloy containing U, Pu, Np, Am, Zr and rare-earth elements, Journal of Nuclear Materials 448(1) (2014) 109-112.
[28] Y.S. Kim, G.L. Hofman, S.L. Hayes, Y.H. Sohn, Constituent redistribution in U–Pu–Zr fuel during irradiation, Journal of Nuclear Materials 327(1) (2004) 27-36.
[29] G.L. Hofman, S.L. Hayes, M.C. Petri, Temperature gradient driven constituent redistribution in U琙Zr alloys, Journal of Nuclear Materials 227(3) (1996) 277-286.
[30] R. Pahl, D. Porter, C. Lahm, G. Hofman, Experimental studies of U-Pu-Zr fast reactor fuel pins in the experimental breeder reactor-ll, Metallurgical Transactions A 21(7) (1990) 1863-1870.
[31] J.M. Harp, D.L. Porter, B.D. Miller, T.L. Trowbridge, W.J. Carmack, Scanning electron microscopy examination of a Fast Flux Test Facility irradiated U-10Zr fuel cross section clad with HT-9, Journal of Nuclear Materials 494 (2017) 227-239.
[32] L. Capriotti, S. Brémier, K. Inagaki, P. Pöml, D. Papaioannou, H. Ohta, T. Ogata, V. Rondinella, Characterization of metallic fuel for minor actinides transmutation in fast reactor, Progress in Nuclear Energy 94 (2017) 194-201.
[33] T. Yao, A.R. Wagner, X. Liu, A. Ei-Azab, J.M. Harp, J. Gan, D.H. Hurley, M.T. Benson, L. He, On spinodal-like phase decomposition in U–50Zr alloy, Materialia 9 (2020) 100592.
[34] J. Rest, Kinetics of fission-gas-bubble-nucleated void swelling of the alpha-uranium phase of irradiated U-Zr and U-Pu-Zr fuel, Journal of Nuclear Materials 207 (1993) 192-204.
[35] P.G. Medvedev, BISON Investigation of the Effect of the Fuel-Cladding Contact Irregularities on the Peak Cladding Temperature and FCCI Observed in AFC-3A Rodlet 4, Idaho National Lab.(INL), Idaho Falls, ID (United States), 2016.
[36] S. Ahn, S. Irukuvarghula, S.M. McDeavitt, Microstructure of α-U and δ-UZr2 phase uranium–zirconium alloys irradiated with 140-keV He+ ion-beam, Journal of Alloys and Compounds 681 (2016) 6-11.
[37] B. Hudson, The crystallography and burgers vectors of dislocation loops in α-uranium, The Philosophical Magazine: A Journal of Theoretical Experimental and Applied Physics 10(108) (1964) 949-960.
[38] T. Yao, B. Gong, L. He, Y. Miao, J.M. Harp, M. Tonks, J. Lian, In-situ TEM study of the ion irradiation behavior of U3Si2 and U3Si5, Journal of Nuclear Materials 511 (2018) 56-63.
[39] J. Gan, D.D. Keiser, B.D. Miller, D.M. Wachs, T.R. Allen, M. Kirk, J. Rest, Microstructure of RERTR DU-alloys irradiated with krypton ions up to 100dpa, Journal of Nuclear Materials 411(1) (2011) 174-180.
[40] T. Yao, A. Wagner, X. Liu, A. Ei-Azab, J. Harp, J. Gan, D.H. Hurley, M.T. Benson, L. He, On Spinodal-like Phase Decomposition in U-50 Zr Alloy, Materialia (2020) 100592.